

MAGNETOHYDRODYNAMIC SIMULATIONS OF ACCRETION ONTO A STAR IN THE “PROPELLER” REGIME

M. M. ROMANOVA

Department of Astronomy, Cornell University, Ithaca, NY 14853-6801; romanova@astro.cornell.edu

O. D. TOROPINA

Space Research Institute, Russian Academy of Sciences, Profsoyuznaya 84/32, Moscow 117997, Russia; toropina@mx.iki.rssi.ru

YU. M. TOROPIN

CQG International Ltd., 10/5 Sadovaya-Karetnaya, Building 1, Moscow 103006, Russia; yuriy@cqg.com

AND

R. V. E. LOVELACE

Department of Astronomy, Cornell University, Ithaca, NY 14853-6801; rv11@cornell.edu

Received 2002 September 14; accepted 2003 January 3

ABSTRACT

This work investigates spherical accretion onto a rotating magnetized star in the “propeller” regime using axisymmetric resistive magnetohydrodynamic simulations. In this regime accreting matter tends to be expelled from the equatorial region of the magnetosphere where the centrifugal force on matter corotating with the star exceeds the gravitational force. The regime is predicted to occur if the magnetospheric radius is larger than the corotation radius and less than the light cylinder radius. The simulations show that accreting matter is expelled from the equatorial region of the magnetosphere and that it moves away from the star in a supersonic, disk-shaped outflow. At larger radial distances the outflow slows down and becomes subsonic. The equatorial matter outflow is initially driven by the centrifugal force, but at larger distances the pressure gradient force becomes significant. We find that the star is spun down mainly by the magnetic torques at its surface with the rate of loss of angular momentum \dot{L} proportional to $-\Omega_*^{1.3}\mu^{0.8}$, where Ω_* is the star’s rotation rate and μ is its magnetic moment. Further, we find that \dot{L} is approximately independent of the magnetic diffusivity of the plasma η_m for a factor ~ 30 range of this parameter, which corresponds to a range of magnetic Reynolds numbers ~ 1 to $\gg 1$. The fraction of the Bondi accretion rate that accretes to the surface of the star is found to be $\propto \Omega_*^{-1.0}\mu^{-2.1}\eta_m^{0.7}$. Predictions of this work are important for the observability of isolated old neutron stars and for wind-fed pulsars in X-ray binaries.

Subject headings: accretion, accretion disks — magnetic fields — plasmas — stars: magnetic fields — X-rays: stars

1. INTRODUCTION

Rotating magnetized neutron stars pass through different stages in their evolution (e.g., Shapiro & Teukolsky 1983; Lipunov 1992). Initially, a rapidly rotating ($P \lesssim 1$ s) magnetized neutron star is expected to be active as a radio pulsar. The star spins down owing to the wind of magnetic field and relativistic particles from the region of the light cylinder r_L (Goldreich & Julian 1969). However, after the neutron star spins down sufficiently, the light cylinder radius becomes larger than the magnetospheric radius, r_m , where the ram pressure of external matter equals the magnetic pressure in the neutron star’s dipole field. The relativistic wind is then suppressed by the inflowing matter (Shvartsman 1970). The external matter may come from the wind from a binary companion or from the interstellar medium for an isolated neutron star. The centrifugal force in the equatorial region at r_m is much larger than gravitational force if r_m is much larger than the corotation radius r_{cor} . In this case the incoming matter tends to be flung away from the neutron star by its rotating magnetic field. This is the so-called “propeller” stage of evolution (Davidson & Ostriker 1973; Illarionov & Sunyaev 1975).

The propeller stage of evolution, though important, is still not well understood theoretically. Different studies have found different dependences for the spin-down rate of the star (Illarionov & Sunyaev 1975; Davies, Fabian, & Pringle

1979; Davies & Pringle 1981; Wang & Robertson 1985; Lipunov 1992). Observational signs of the propeller stage have been discussed by a number of authors (e.g., Stella, White, & Rosner 1986; Treves & Colpi 1991; Cui 1997; Treves et al. 2000). The rapid spin-down of strongly magnetized stars (i.e., magnetars) in the pulsar and propeller stages of evolution may give relatively young isolated neutron stars without detectable pulsations (M. Ruderman 2002, private communication). Walter & Lattimer (2002) give new astrometric evidence that the isolated neutron star RX J185635–3754 has an age $\sim 5 \times 10^6$ yr but gives no evidence of pulsations.

MHD simulations of disk accretion onto a rotating star in the propeller regime were done by Wang & Robertson (1985). However, the authors considered only the equatorial plane and concentrated on investigation of instabilities at the boundary between the magnetosphere and the surrounding medium. Thus, they could not investigate accretion along the magnetic poles of the star. An analytical model of disk accretion in the propeller regime was developed by Lovelace, Romanova, & Bisnovaty-Kogan (1999). Disk accretion at the stage of weak propeller ($r_m \sim r_{\text{cor}}$) was investigated numerically by Romanova et al. (2002).

The mentioned studies obtained possible trends of the propeller stage of evolution. However, two- and three-dimensional MHD simulations are needed to obtain more definite answers to the important physical questions. The

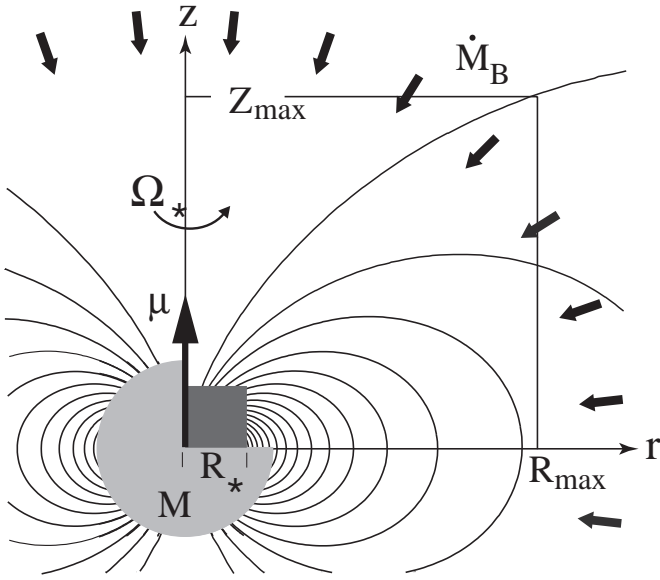


FIG. 1.—Geometry of the MHD simulation region, where \dot{M}_B is the Bondi accretion rate, μ and Ω_* are the magnetic moment and angular velocity of the star, R_* is the radius of the star, and (R_{\max}, Z_{\max}) are the limits of the computational region. In the described calculations $R_* \ll R_{\max}$.

questions that need to be answered are the following: (1) What are the physical conditions of the matter flow around the star in the propeller regime of accretion? (2) What is the spin-down rate of the star, and how does it depend on the star's magnetic moment and rotation rate and on the inflow rate of the external matter? (3) What is the accretion rate to the surface of the star and how does it depend on the star's rotation rate and magnetic moment? (4) What are the possible observational consequences of this stage of evolution?

This paper discusses results of axisymmetric, two-dimensional, resistive MHD simulations of accretion onto a rotating magnetized star in the propeller regime. The situation is shown in Figure 1. We treat the case in which matter accretes spherically with the Bondi accretion rate. Bondi accretion onto a nonrotating and a slowly rotating star was investigated by Toropin et al. (1999, hereafter T99). It was shown that the magnetized star accretes matter at a rate less than the Bondi rate. Toropina et al. (2003, hereafter T03) confirmed this result for stronger magnetic fields. In this paper we consider initial conditions similar to those in T03, but investigate the case of rapidly rotating stars. Section 2 gives a rough physical treatment of the propeller regime. Section 3 describes the numerical model and computations. Section 4 describes the main results from our simulations, and § 5 gives a numerical application of our results. Section 6 gives the conclusions from this work.¹

2. PHYSICS OF THE PROPELLER REGIME

In the propeller regime the magnetospheric radius r_m is larger than the corotation radius $r_{\text{cor}} = (GM/\Omega_*^2)^{1/3} \approx 0.78 \times 10^9 P_{10}^{2/3}$ cm, and incoming matter in the equatorial plane is flung away from the star. Here we assume $M = 1.4 M_\odot$, and $P_{10} = P/10$ s, with P the rotation period of the star. The magnetospheric radius is determined by a balance of the ram pressure of the inflowing matter $p_m + \rho_m v_m^2$

against the magnetic pressure $B^2/8\pi$ of the neutron star's field $B_m = \mu/r_m^3$, where the m subscripts indicate that the quantity is evaluated at a distance r_m , and μ is the star's magnetic moment.

Consider first the case of a nonrotating star. The Bondi inflow velocity at r_m is supersonic for specific heat ratios $\gamma < 5/3$. Thus $\rho_m = \dot{M}/[4\pi(1-f)r_m^{3/2}\sqrt{GM}]$, where \dot{M} is the accretion rate, and $1-f$ is the fraction of the solid angle in which there is inflow. For this case the ram pressure is approximately $\rho_m GM/r_m$, so that

$$r_{m0} = \left[\frac{\mu^2}{2(1-f)\dot{M}\sqrt{GM}} \right]^{2/7} \approx 6.1 \times 10^{10} \left[\frac{\mu_{30}^2}{(1-f)\dot{M}_{-17}} \right]^{2/7} \text{ cm} \quad (1)$$

(Davidson & Ostriker 1973; Shapiro & Teukolsky 1983). Here, $\mu_{30} = \mu/10^{30}$ G cm³ and $\dot{M}_{-17} = \dot{M}/10^{-17} M_\odot \text{ yr}^{-1}$.

For a rapidly rotating star ($r_m \gg r_{\text{cor}}$), the dominant velocity is due to the rotation of the magnetosphere so that $v_m^2 = (\Omega_* r_m)^2$. The flow velocity is much larger than the sound speed so that this is a ‘‘supersonic propeller’’ (Davies et al. 1979). Neglecting the complicated two-dimensional nature of the plasma flow, we estimate $\rho'_m (\Omega_* r_m)^2 \approx \mu^2 / (8\pi r_m^6)$, where ρ'_m is the density of the outflowing matter, which moves away from the star at a speed $\approx \Omega_* r_m$ in a solid angle $4\pi f$ so that $\rho'_m = \dot{M} / (4\pi f r_m^2 \Omega_* r_m)$. This gives

$$r_{m\Omega} \approx \left(\frac{\mu^2 f}{2\dot{M}\Omega_*} \right)^{1/5} \approx 1.3 \times 10^{10} \left(\frac{\mu_{30}^2 f_{0.3} P_{10}}{\dot{M}_{-17}} \right)^{1/5} \text{ cm} \quad (2)$$

(Wang & Robertson 1985; R. V. E. Lovelace, M. M. Romanova, & G. S. Bisnovatyi-Kogan 2003, in preparation), where $f_{0.3} = f/0.3$. In this limit, there is to a first-order approximation no accretion onto the star; all of the incoming matter is flung away from the star in the equatorial plane by the rotating magnetic field.

Equations (1) and (2) give the same values for $\Omega_2 = (2\dot{M}/\mu^2)^{3/7} (GM)^{5/7} f(1-f)^{10/7}$, which corresponds to a period $P_2 \approx 3.9 \times 10^4 (\mu_{30}^2 / \dot{M}_{-17})^{3/7}$ s for $f = 0.3$. The propeller regime requires periods $P < P_2$. At the other extreme, the condition that $r_{m\Omega}$ be less than the light cylinder radius gives the condition $\Omega_* > \Omega_1 = [2Mc^5/(\mu^2 f)]^{1/4}$ or $P > P_1 \approx 2(\mu_{30}^2 f_{0.3} / \dot{M}_{-17})^{1/4}$ s.

The spin-down rate of the star can be estimated as $I d\Omega_*/dt \approx 4\pi r_m^2 f (r_m B_m^2 / 8\pi)$, which is the magnetic torque at the radius r_m . This assumes that $B_\phi \approx B_m$ at r_m . Thus,

$$I \frac{d\Omega_*}{dt} \approx - \frac{\mu^2 f}{2r_{m\Omega}^3} = -0.76 \mu^{4/5} f^{2/5} \Omega_*^{3/5} \dot{M}^{3/5} \quad (3)$$

This gives a spin-down timescale

$$\tau = \frac{\Omega_*}{|d\Omega_*/dt|} \approx \frac{3 \times 10^8 \text{ yr}}{\mu_{30}^{4/5} \dot{M}_{-17}^{3/5} f_{0.3}^{2/5} P_{10}^{2/5}},$$

where the neutron star's moment of inertia I is assumed to be 10^{45} g cm². The angular momentum lost by the star goes into outflow of material mainly in the equatorial plane. The rotational power lost by the star, $I\Omega_* d\Omega_*/dt$, goes into the kinetic (thermal plus flow) energy of the equatorial outflow.

¹ Animation of the propeller outflows is given at <http://www.astro.cornell.edu/us-russia/propeller.htm>.

Note that the time for the pulsar to spin down from its initial period (assumed $\ll P_1$) to P_1 owing to the Goldreich-Julian torque (where $\dot{P} \propto 1/P$) is

$$t_{01} = \frac{I}{\mu} \left(\frac{2cf}{\dot{M}} \right)^{1/2} \approx 1.7 \times 10^8 \frac{I_{45}}{\mu_{30}} \left(\frac{f_{0.3}}{\dot{M}_{-17}} \right)^{1/2} \text{ yr}.$$

On the other hand, the time for the pulsar to spin down from a period P_1 to a period $\gg P_1$ due to the propeller torque of equation (3) (where $\dot{P} \propto P^{7/5}$) is

$$t_{1\infty} = \frac{5I}{2\mu} \left(\frac{2c}{\dot{M}f} \right)^{1/2} \approx 1.4 \times 10^9 \frac{I_{45}}{\mu_{30} f_{0.3}^{1/2} \dot{M}_{-17}^{1/2}} \text{ yr}.$$

Note that $t_{1\infty}$ exceeds t_{01} by a factor of $5/(2f)$.

3. NUMERICAL MODEL

We simulate the plasma flow in the propeller regime using an axisymmetric resistive MHD code. The code incorporates the methods of local iterations and flux-corrected transport (Zhukov, Zabrodin, & Feodoritova 1993). The code is described in our earlier investigation of Bondi accretion onto a nonrotating magnetized star (T99). The equations for resistive MHD are

$$\frac{\partial \rho}{\partial t} + \nabla \cdot (\rho \mathbf{v}) = 0, \quad (4)$$

$$\rho \frac{\partial \mathbf{v}}{\partial t} + \rho (\mathbf{v} \cdot \nabla) \mathbf{v} = -\nabla p + \frac{1}{c} \mathbf{J} \times \mathbf{B} + \mathbf{F}^g, \quad (5)$$

$$\frac{\partial \mathbf{B}}{\partial t} = \nabla \times (\mathbf{v} \times \mathbf{B}) + \frac{c^2}{4\pi\sigma} \nabla^2 \mathbf{B}, \quad (6)$$

$$\frac{\partial (\rho \varepsilon)}{\partial t} + \nabla \cdot (\rho \varepsilon \mathbf{v}) = -p \nabla \cdot \mathbf{v} + \frac{\mathbf{J}^2}{\sigma}. \quad (7)$$

We assume axisymmetry ($\partial/\partial\phi = 0$) but calculate all three components of \mathbf{v} and \mathbf{B} . The equation of state is taken to be that for an ideal gas, $p = (\gamma - 1)\rho\varepsilon$, with specific heat ratio $\gamma = 7/5$. A value of γ less than $5/3$ is expected in the case of an ionized gas because of the influence of the electron heat conduction. The equations incorporate Ohm's law $\mathbf{J} = \sigma(\mathbf{E} + \mathbf{v} \times \mathbf{B}/c)$, where σ is the electrical conductivity. The associated magnetic diffusivity, $\eta_m \equiv c^2/(4\pi\sigma)$, is considered to be a constant within the computational region. In equation (5) the gravitational force, $\mathbf{F}^g = -GM\rho\mathbf{R}/R^3$, is due to the central star.

We use a cylindrical, inertial coordinate system (r, ϕ, z) with the z -axis parallel to the star's dipole moment $\boldsymbol{\mu}$ and rotation axis Ω . The equatorial plane is treated as a symmetry plane. The vector potential \mathbf{A} is calculated so that $\nabla \cdot \mathbf{B} = 0$ at all times. The full set of equations is given in T99.

The star rotates with angular velocity $\Omega_* = \Omega_* \hat{\mathbf{z}}$. It is useful to introduce the dimensionless quantity $\omega_* \equiv \Omega_*/\Omega_{K*} \leq 1$, where $\Omega_{K*} = (GM/R_*^3)^{1/2}$ is the Keplerian angular velocity at the stellar radius R_* . Simulations have been done for different values of $\omega_* = 0-0.7$. The intrinsic magnetic field of the star is taken to be an aligned dipole, $\mathbf{B} = [3\mathbf{R}(\boldsymbol{\mu} \cdot \mathbf{R}) - R^2\boldsymbol{\mu}]/R^5$ with $\boldsymbol{\mu} = \mu\hat{\mathbf{z}}$ and vector potential $\mathbf{A} = \boldsymbol{\mu} \times \mathbf{R}/R^3$.

To convert our equations to dimensionless form we measure length in units of the Bondi radius $R_B \equiv GM/c_\infty^2$, with c_∞ the sound speed at infinity, density in units of the density

at infinity ρ_∞ , and magnetic field strength in units of B_0 , which is the field at the pole of the numerical star ($r = 0$, $z = Z_*$). Pressure is measured in units of $B_0^2/8\pi$. The magnetic moment is measured in units of $\mu_0 = B_0 R_B^3/2$. We measure velocity in units of the Alfvén speed $v_0 = B_0(4\pi\rho_\infty)^{-1/2}$. However, in the plots we give the velocities in units of c_∞ .

After putting equations (4)–(7) in dimensionless form, one finds three dimensionless parameters, two of which are

$$\beta \equiv \frac{8\pi p_\infty}{B_0^2}, \quad \tilde{\eta}_m \equiv \frac{\eta_m}{R_B v_0} = \frac{1}{S_0}. \quad (8)$$

Here, $\tilde{\eta}_m$ is the dimensionless magnetic diffusivity, which may be interpreted as the reciprocal of a fiducial Lundquist number S_0 , and $p_\infty = \rho c_\infty^2/\gamma$ is the pressure at infinity. The third parameter, $g = GM/(R_B v_0^2) = \gamma\beta/2$, is on the order of β . We also use a parameter b_0 to control the field strength of the star. It is defined by the equation $\mathbf{A} = b_0 \mathbf{A}_0$, where b_0 has been varied in the range 1–25.

Simulations were done in a cylindrical “can” ($0 \leq z \leq Z_{\max}$, $0 \leq r \leq R_{\max}$). The size of the region was taken to be $R_{\max} = Z_{\max} = R_s/\sqrt{2} = R_B/5\sqrt{2} \approx 0.141R_B$, which is less than the sonic radius of the Bondi flow $R_s = [(5 - 3\gamma)/4]R_B = 0.2R_B$ ($\gamma = 7/5$). Thus, matter inflows supersonically to the computational region. The inflow rate is taken to be the Bondi (1952) accretion rate, $\dot{M}_B = 4\pi\lambda(GM_*)^2\rho_\infty/c_\infty^3$, where $\lambda = 0.625$ for $\gamma = 7/5$. The incoming matter is assumed to be unmagnetized. A uniform (r, z) grid with $N_R \times N_Z$ cells was used. For the results discussed here $N_R \times N_Z = 513 \times 513$.

The “numerical star” is taken to be a cylinder of radius R_* and half-axial length Z_* with $R_* = Z_* \ll R_{\max}$, Z_{\max} . In the results presented here, $R_* = Z_* = 0.0044R_B$. Clearly, the numerical star is very large: the value of R_*/R_B , although much less than unity, is much larger than the astrophysical ratio for a neutron star ($\sim 10^{-4}$). The grid size, $DR = R_{\max}/N_R = 2.76 \times 10^{-4}R_B$, is about 16 times smaller than the star's radius.

Initial conditions.—Initially, the density $\rho(r, z)$ and the velocity $\mathbf{v}(r, z)$ are taken to be the values given by the Bondi (1952) solution with $\gamma = 7/5$. Thus, initially $v_\phi = 0$. Also, initially the vector potential \mathbf{A} is taken as that of a dipole so that $B_\phi = 0$. The star is initialized to be rotating at the rate Ω_* .

Boundary conditions.—At the outer boundaries, $r = R_{\max}$ and $z = Z_{\max}$, the variables $(\rho, v_r, v_z, \varepsilon)$ are fixed and equal to the values for the Bondi flow, which has $v_\phi = 0$. The inflowing matter is unmagnetized with $\mathbf{B} = 0$. At the inner boundary, the vector potential $\mathbf{A} = \hat{\boldsymbol{\phi}} A_\phi$ of the intrinsic dipole field of the star is determined on the surface of the model star. The value of the vector potential on this surface is fixed, corresponding to the star's being a perfect conductor. Equivalently, the component of the \mathbf{B} field normal to the surface is fixed, but the other two components vary. The density and internal energy at the inner boundary are set equal to small numerical values. Thus, incoming matter with higher values of these parameters is absorbed by the star. This treatment of the star is analogous to that used by Ruffert (1994a, 1994b). Typically, the density of incoming matter is $\gtrsim 10^3$ times larger than the density inside the star $\rho = 1$. For a purely hydrodynamic spherical accretion flow with no rotation, we verified that this accretor absorbs all incoming matter at the Bondi rate.

4. MATTER FLOW IN THE PROPELLER REGIME

Here, we first discuss simulations for the case $\omega_* = 0.5$, $\beta = 10^{-7}$, magnetic diffusivity $\tilde{\eta}_m = 10^{-5}$ (eq. [8]), and field strength $b_0 = 10$. At the end of this section we discuss the dependence of the results on ω_* , $\mu(b_0)$, and η_m .

Time is measured in units of the free-fall time from the top or the side of the simulation region, $t_{\text{ff}} = Z_{\text{max}}/v_{\text{ff}}$, with $v_{\text{ff}} = (2GM/Z_{\text{max}})^{1/2}$. For the rotating star, time is also given in terms of rotation periods of the star, $P_* = 2\pi/\Omega_*$.

For the mentioned values of β , b_0 , and η_m , the magnetospheric radius r_{m0} and corotation radius $r_{\text{cor}} = (GM/\Omega_*^2)^{1/3}$ are equal for $\omega_* \approx 0.16$. For smaller angular velocities, $\omega_* < 0.16$, the matter flow around the star is close to that in the nonrotating case. For $\omega_* > 0.16$ the flow exhibits the features expected in the propeller regime.

Figures 2 and 3 show the general nature of the flow in the propeller regime. Two distinct regions separated by a shock wave are observed: One is the *external* region, where matter inflows with the Bondi rate, and the density and velocity agree well with the Bondi (1952) solution. The second is the *internal* region, where the flow is strongly influenced by the stellar magnetic field and rotation. The shock wave, which divides these regions, propagates outward as in the nonrotating case (T99). For a rotating star in the propeller regime the shock wave has the shape of an ellipsoid flattened along the rotation axis of the star.

The region of the flow well within the shock wave is approximately time independent. The accretion rate onto the star becomes constant after about 1–2 rotation periods of the star.

A new regime of matter flow forms inside the expanding shock wave. The rapidly rotating magnetosphere expels matter outward in the equatorial region. This matter flows radially outward, forming a low-density rotating torus. The outflowing matter is decelerated when it reaches the shock wave. There, the flow changes direction and moves toward the rotation axis of the star. However, only a small fraction of this matter accretes onto the surface of the star. Most of the matter is expelled again in the equatorial direction by the rotating field of the star. Thus, most of the matter circulates inside this inner region, driven by the rapidly rotating magnetosphere. Large-scale vortices form above and below the equatorial torus (see Figs. 2 and 3). In three dimensions vortices of smaller scale may also form. Thus, at the propeller stage the significant part of the rotational energy of the star may go into the directed and thermal energy of the expelled plasma.

The solid line in Figure 3 shows the Alfvén surface, where the magnetic energy density equals the thermal plus kinetic energy density, $B^2/8\pi = \varepsilon + \rho v^2/2$. In the equatorial plane, the Alfvén radius is $r_A \approx 4.5R_*$. For $r < r_A$, the magnetic pressure dominates, and the magnetic field is approximately that of a dipole. At larger distances the field is stretched by the outflowing plasma. Matter inside the magnetopause (the region of closed magnetic field lines inside the Alfvén surface) rotates with the angular velocity of the star (see Fig. 4). For $r > r_A$, matter continues to rotate in the equatorial region but the angular velocity decreases with r . Figure 5a shows the radial variation of the velocities in the equatorial plane. Matter is accelerated by the rotating magnetosphere for $r > 4R_*$ up to $r \sim 10R_*$, but at larger

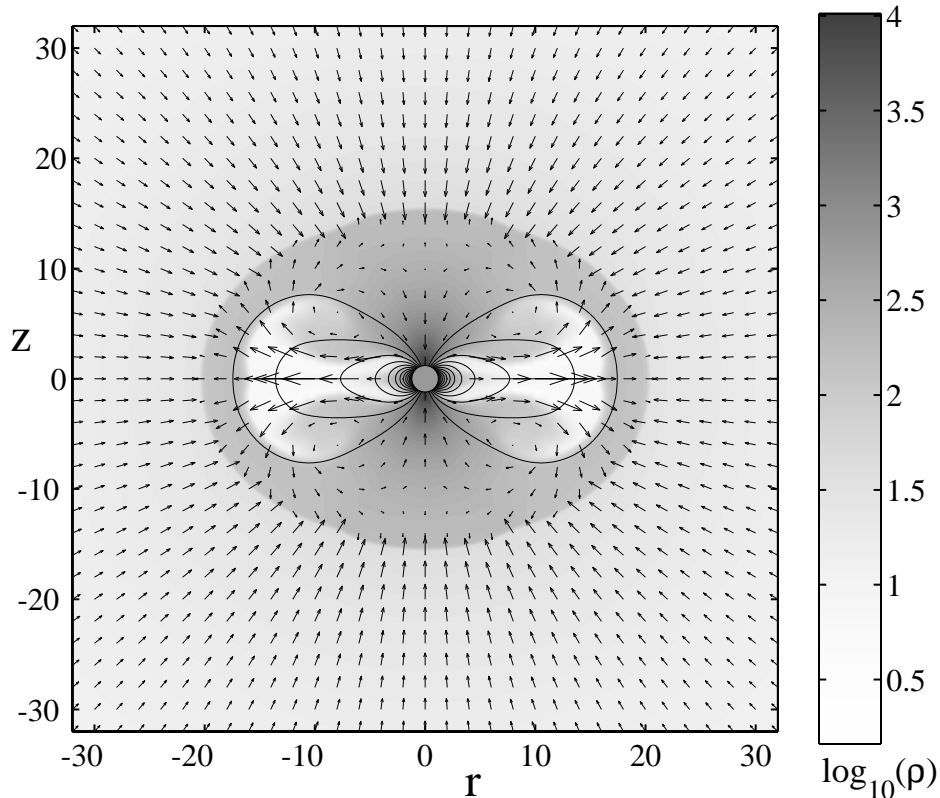


FIG. 2.—Matter flow in the propeller regime for a star rotating at $\Omega_* = 0.5\Omega_{K*}$ after 6.9 rotation periods of the star. The axes are measured in units of the star's radius. The background shading represents the density, and the length of the arrows is proportional to the poloidal velocity. The thin solid lines are magnetic field lines.

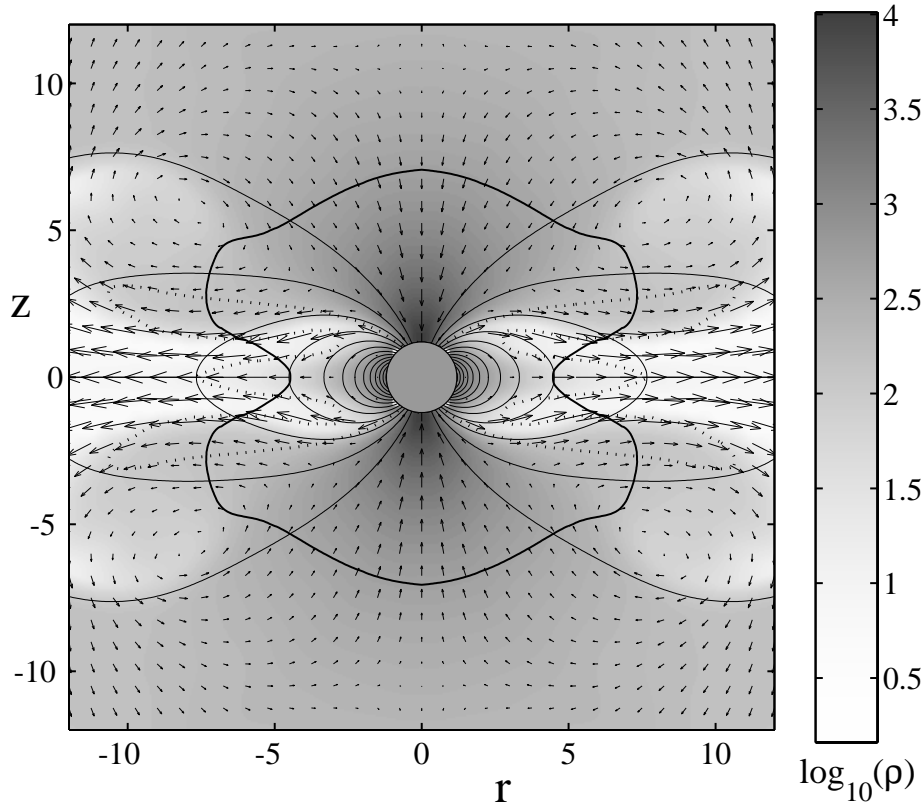


FIG. 3.—Enlarged view of Fig. 2. The bold line represents the Alfvén surface. Dotted line shows sonic surface. The axes are measured in units of stellar radii R_* .

distances the radial velocity decreases. The azimuthal velocity v_ϕ is significantly larger than the radial velocity at $r \sim 4R_*$, but they become equal at larger distances. The sound speed c_s is high inside the shock wave owing to the Joule heating J^2/σ . Nevertheless, the outflow is supersonic in the region $r \sim (4-7)R_*$. Note that above and below the

equatorial plane the region of the supersonic outflow is larger (see sonic surface line in Figs. 3 and 4). Figure 5b shows the variation of the velocities along the z -axis.

Figure 6 shows the streamlines of the matter flow. Matter free-falls along the field lines going into the poles of the star. Some matter that flows close to the z -axis accretes onto the surface of the star. However, matter more remote from the z -axis comes close to the star, is deflected by the rotating magnetic field, and then moves outward in the equatorial plane.

Figure 7 shows the radial dependences of the different radial forces in the equatorial plane. One can see that for $r > 3.7R_*$, the centrifugal force becomes dominant in accelerating the matter outward. However, at larger distances ($r > 5.5R_*$), the pressure gradient force becomes larger and determines acceleration of matter. Thus, centrifugal and pressure gradient forces accelerate matter in the radial direction. Note that in most of the region ($r > 4.3R_*$) the magnetic force is negative, so that it opposes the matter outflow.

The results we have shown are for a relatively strong propeller. If the rotation rate is smaller, then the matter outflow become less intense. For $\omega_* < 0.16$, no equatorial outflow is observed, and the shock wave becomes nearly spherical, as it is in the nonrotating case. Conversely, the shock wave becomes a more and more flattened ellipsoid for larger ω_* . Matter rotates rigidly inside the Alfvén radius r_A , while at large distances $\Omega = v_\phi/r$ decreases. Figure 8 shows the radial dependences of the angular velocity in the equatorial plane for different values of ω_* .

Figure 9a shows that the accretion rate onto the star decreases as the angular velocity of the star increases, $\dot{M}/\dot{M}_B \propto \omega_*^{-1.0}$. Figure 9b shows that the accretion rate

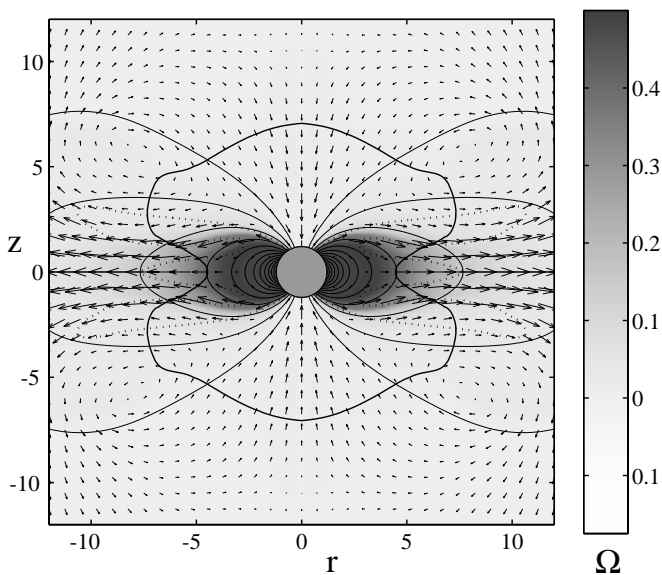


FIG. 4.—Same as on Fig. 3, but the background shading represents angular velocity $\Omega = v_\phi(r, z)/r$. The axes are measured in units of stellar radii R_* .

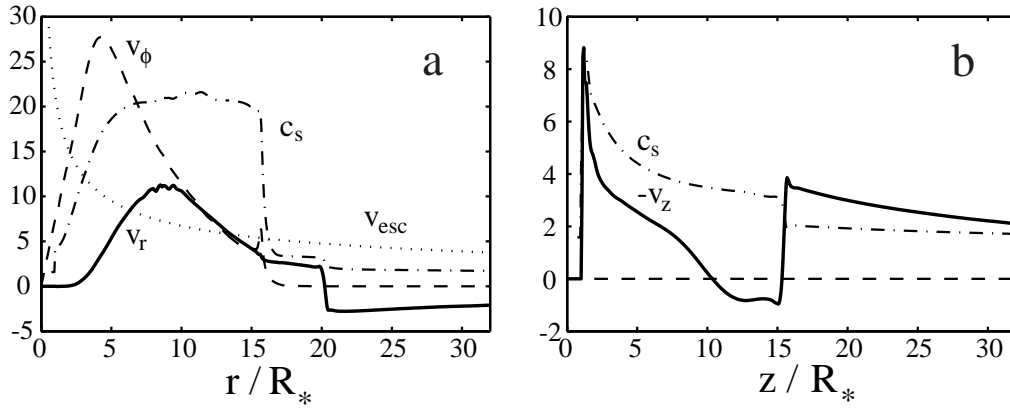


FIG. 5.—(a) Radial variation at $z = 0$ of the azimuthal velocity v_ϕ , the radial velocity v_r , the sound speed c_s , and the escape velocity v_{esc} , all in units of c_∞ . (b) Variation of the velocities along the z -axis. The fact that the sign of the flow velocity changes across the shock is due to the shock's outward velocity.

onto the star decreases as the star's magnetic moment increases: $\dot{M}/\dot{M}_B \propto \mu^{-2.1}$. We have also done a number of simulation runs for different magnetic diffusivities in the range $\tilde{\eta}_m = 10^{-6}$ – $10^{-4.5}$, and from this we conclude that $\dot{M}/\dot{M}_B \propto (\eta_m)^{0.7}$. Accretion along the rotation axis of stars in the propeller regime was discussed by Nelson, Salpeter, & Wasserman (1993). Three-dimensional instabilities (e.g., Arons & Lea 1976) not included in the present two-dimensional simulations may act to increase the accretion rate to the star's surfaces.

Figure 10 shows the total angular momentum loss rate from the star as a function of ω_* . This was obtained by evaluating the integral

$$\dot{L} = - \int dS \cdot \left(\rho v_p r v_\phi - \frac{B_p r B_\phi}{4\pi} \right) \quad (9)$$

over the surface of the numerical star. Here dS is the outward pointing surface area element and the p subscript indicates the poloidal component. The dominant contribution

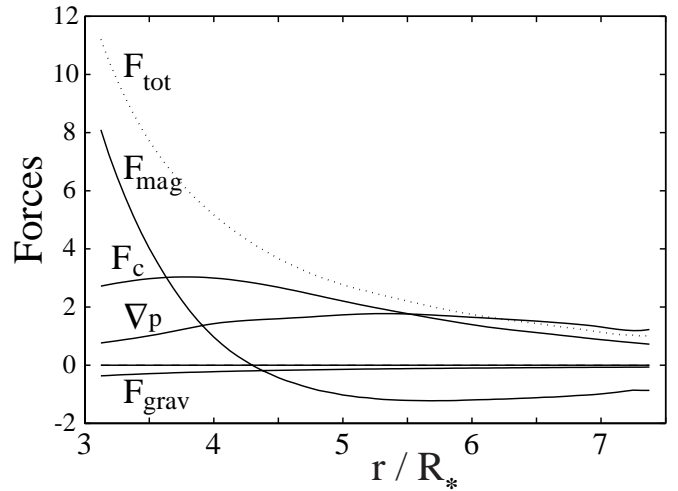


FIG. 7.—Radial dependence of the different radial forces acting in the equatorial plane; $F_{mag} = (\mathbf{J} \times \mathbf{B})_r / c$ is the magnetic force (per unit volume), $F_c = \rho v_\phi^2 / r$ is the centrifugal force, $\nabla p = (\nabla p)_r$ is minus the pressure gradient force, $F_{grav} = -\rho(\nabla\Phi_{grav})_r$ is the gravitational force, and F_{tot} is the total radial force. The vertical scale is arbitrary. The centrifugal force is the dominant one that drives matter to the centrifugal equatorial wind.

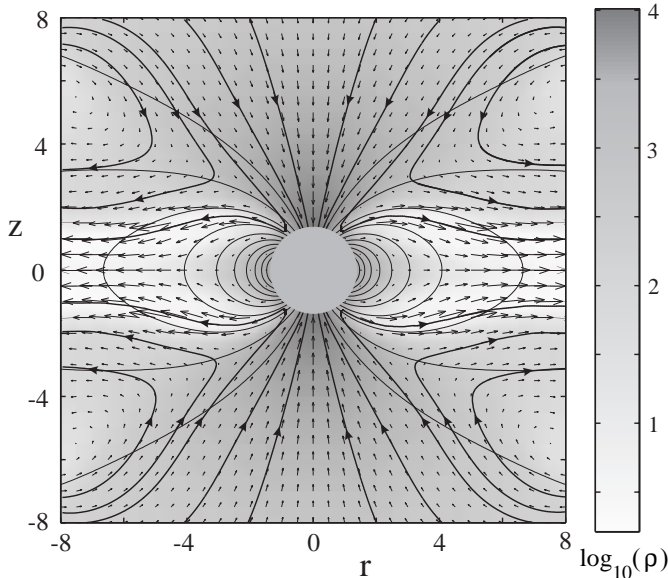


FIG. 6.—Same as Fig. 3, but bold solid lines are added, which show the streamlines of the matter flow.

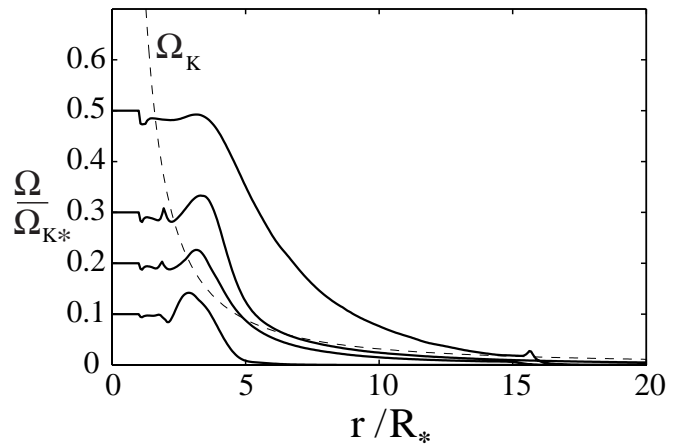


FIG. 8.—Angular velocity of matter $\Omega = v_\phi / r$ vs. r in the equatorial region for different angular velocities of the star. The dashed line represents the Keplerian angular velocity $\Omega_K = (GM/r^3)^{1/2}$.

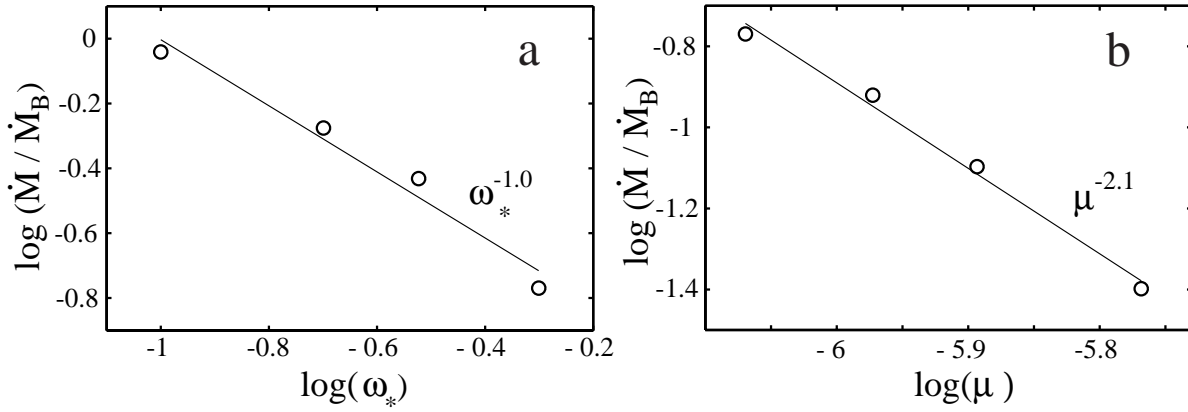


FIG. 9.—(a) Fraction of Bondi accretion rate reaching the star as a function of the star’s angular velocity $\omega_* = \Omega_*/\Omega_{K*}$. For a nonrotating star, $\dot{M}/\dot{M}_B = 0.07$ or $\log(\dot{M}/\dot{M}_B) = -1.1$. (b) Dependence on the magnetic moment μ for $\omega_* = 0.5$. The straight lines show the approximate power-law dependences.

to equation (9) is the magnetic field term, and this term increases relative to the matter term as Ω_* increases. The dependence predicted by equation (3), $\dot{L} \propto -\Omega_*^{3/5}$, is shown by the dashed line. The fact that the observed dependence, $\dot{L} \propto -\Omega_*^{1.3}$, is steeper may be due to the fact that the magnetospheric radius is not much larger than the corotation radius. Also, we find that $\dot{L} \propto -\mu^{0.8}$ for a factor of 4 range of μ about our main case. From simulation runs with magnetic diffusivities in the range $\tilde{\eta}_m = 10^{-6}$ – $10^{-4.5}$, we conclude that \dot{L} depends very weakly on the magnetic diffusivity, $\dot{L} \propto -(\eta_m)^{-0.1}$.

5. ASTROPHYSICAL EXAMPLE

Here we give the conversions of the dimensionless variables to physical values for the case $\beta = 10^{-7}$, $b_0 = 10$, and $\tilde{\eta}_m = 10^{-6}$ (eq. [8]). We consider accretion onto a magnetized star with mass $M = 1.4 M_\odot = 2.8 \times 10^{33}$ g. The density of the ambient interstellar matter is taken to be $\rho_\infty = 1.7 \times 10^{-24}$ g cm $^{-3}$ ($n_\infty = 1$ cm $^{-3}$). We consider a higher than typical sound speed in the ISM, $c_\infty = 100$ km s $^{-1}$, in order to have a smaller Bondi radius compatible with our simulations. (Notice also that a large sound speed pro-

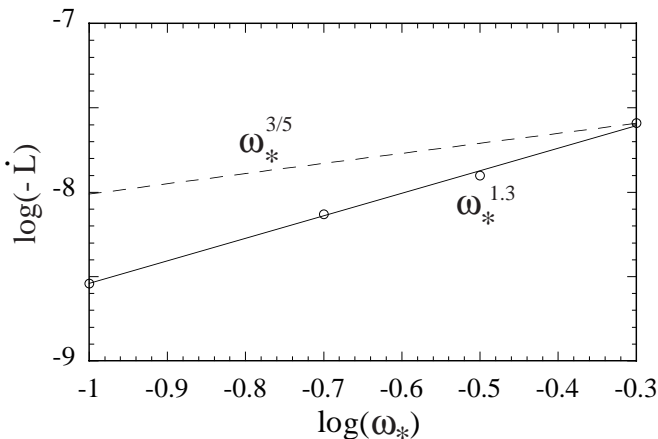


FIG. 10.—Total angular momentum outflow from the star as a function of $\omega_* = \Omega_*/\Omega_{K*}$. The straight line is a power-law fit $\dot{L} \propto -(\Omega_*)^{1.3}$. This is steeper than the predicted dependence of eq. (3), $\dot{L} \propto -(\Omega_*)^{3/5}$, which is shown by the dashed line in the figure. The vertical scale is arbitrary.

vides a rough way of modeling accretion onto a neutron star moving supersonically.) The Bondi radius is

$$R_B = GM_*/c_\infty^2 \approx 1.9 \times 10^{12} c_{100}^{-2} \text{ cm} , \quad (10)$$

and the Bondi (1952) accretion rate is

$$\dot{M}_B = 4\pi\lambda(GM_{NS})^2 \rho_\infty/c_\infty^3 \approx 0.7 \times 10^{-17} (n_1/c_{100}^3) M_\odot \text{ yr}^{-1} , \quad (11)$$

where $\lambda = 0.625$ for $\gamma = 1.4$, $n_1 = n_\infty/(1 \text{ cm}^{-3})$, and $c_{100} = c_\infty/(100 \text{ km s}^{-1})$. Using the definitions $\beta = 8\pi p_\infty/B_0^2$, $p_\infty = \rho_\infty c_\infty^2/\gamma$, and the fact that $b_0 = 10$, we obtain the magnetic field at the surface of the “numerical” star $B_* \approx 1.7$ G.

Recall that the size of the numerical star is $R_* = 0.0044R_B \approx 0.82 \times 10^{10}$ cm in all simulations. Thus, the magnetic moment of the numerical star is $\mu = B_* r_*^3/2 \approx 0.48 \times 10^{30}$ G cm 3 . Note that this is of the order of the magnetic moment of a neutron star with surface field 10^{12} G and radius 10^6 cm.

The numerical star rotates with angular velocity $\Omega_* = \omega_* \Omega_{K*}$, where $\Omega_{K*} = (GM/R_*^3)^{1/2}$. For most of the figures $\omega_* = 0.5$, and this corresponds to a period of $P_* = 2\pi/\Omega_* \approx 685$ s.

Using the mass accretion rate of equation (11) and $\mu_{30} = 1$, the magnetospheric radius of the nonrotating star, from equation (1), is $r_{m0} \approx 7.5 \times 10^{10}$ cm $\approx 9R_*$ for $f = 0.3$. The magnetospheric radius of the rotating star with $\omega_* = 0.5$, from equation (2), is $r_{m\Omega} \approx 3.3 \times 10^{10}$ cm $\approx 4R_*$. From Figure 8 note that the equatorial profile of the angular rotation rate $\Omega(r, 0)$ for $\omega_* = 0.5$ is approximately flat out to $r_{\text{flat}} \approx 4.2R_*$, which is roughly the same as $r_{m\Omega}$. As required, the corotation radius, $r_{\text{cor}} = R_*/\omega_*^{2/3} \approx 1.6R_*$, is appreciably less than $r_{m\Omega}$. For smaller values of ω_* in Figure 8, r_{flat} decreases gradually. This dependence on ω_* differs from that of equation (2), which may be due to the fact that $r_{m\Omega}$ is not very large compared with r_{cor} . As ω_* decreases, r_{cor} increases rapidly. Thus the case $\omega_* = 0.1$, where $r_{\text{cor}} > r_{\text{flat}}$, is not in the propeller regime.

For the considered case and $\omega_* = 0.5$, we have evaluated equation (9) numerically with the result that $\dot{L} \approx -4.7 \times 10^{28}$ g cm 2 s $^{-2}$. The theoretical estimate of \dot{L} from equation (3) for the mentioned values of μ and $r_{m\Omega}$ is substantially

smaller, $\dot{L}_{\text{th}} = -0.42 \times 10^{28} \text{ g cm}^2 \text{ s}^{-2}$. A factor of ~ 2.2 reduction of $r_{m\Omega}$ brings \dot{L}_{th} into coincidence with the \dot{L} from the simulations. The difference in the \dot{L} values may result from the fact that $r_{m\Omega}$ is not very large compared with r_{cor} .

For this case with $\omega_* = 0.5$, the magnetic Reynolds number defined as $\text{Re}_m = \Omega_* r_{m\Omega}^2 / \eta_m$ works out to be $\text{Re}_m \approx 140$.

6. CONCLUSIONS

Axisymmetric magnetohydrodynamic simulations of Bondi accretion onto a rotating magnetized star in the propeller regime of accretion have shown the following: (1) A new regime of matter flow forms around a rotating star. Matter falls down along the axis, but only a small fraction of the incoming matter accretes onto the surface of the star. Most of the matter is expelled radially in the equatorial plane by the rotating magnetosphere of the star. A low-density torus forms in the equatorial region that rotates with velocity significantly larger than the radial velocity. Large-scale vortices form above and below the equatorial plane. (2) The star is spun down by the magnetic torque and to a lesser extent the matter torque at its surface. The rate of loss of angular momentum \dot{L} is proportional to $-\Omega_*^{1.3} \mu^{0.8}$, and it is approximately independent of the magnetic diffusivity η_m for a factor of ~ 30 range of this parameter, which corre-

sponds to a range of magnetic Reynolds numbers ~ 1 to $\gg 1$. This dependence differs from the predicted dependence of equation (3) probably because the corotation radius is not much smaller than the magnetospheric radius r_m . The rotational energy lost by the star goes into the directed and thermal energy of plasma. (3) The accretion rate to the star is much less than the Bondi accretion rate and decreases as (a) the star's rotation rate increases ($\propto \Omega_*^{-1.0}$), (b) as the star's magnetic moment increases ($\propto \mu^{-2.1}$), and (c) as the magnetic diffusivity decreases [$\propto (\eta_m)^{0.7}$]. (4) Because the accretion rate to the star is less than the Bondi rate, a shock wave forms in our simulations and propagates outward. It has the shape of an ellipsoid flattened along the rotation axis of the star.

This work was supported in part by NASA grant NAG5-9047, by NSF grant AST-9986936, and by Russian program "Astronomy." M. M. R. is grateful to an NSF POWRE grant for partial support. R. V. E. L. was partially supported by grant NAG5-9735. O. D. T. was partially supported by INTAS grant 01-491. We thank V. V. Savelyev for the development of the original version of the MHD code used in this work and Professor M. Ruderman for valuable discussions. Also, we thank an anonymous referee for helpful criticism.

REFERENCES

- Arons, J., & Lea, S.M. 1976, *ApJ*, 207, 914
 Bondi, H. 1952, *MNRAS*, 112, 195
 Cui, W. 1997, *ApJ*, 482, L163
 Davidson, K., & Ostriker, J. P. 1973, *ApJ*, 179, 585
 Davies, R. E., Fabian, A. C., & Pringle, J. E. 1979, *MNRAS*, 186, 779
 Davies, R. E., & Pringle, J. E. 1981, *MNRAS*, 196, 209
 Goldreich, P., & Julian, W. H. 1969, *ApJ*, 157, 869
 Illarionov, A. F., & Sunyaev, R. A. 1975, *A&A*, 39, 185
 Lipunov, V. M. 1992, *Astrophysics of Neutron Stars* (Berlin: Springer)
 Lovelace, R. V. E., Romanova, M. M., & Bisnovatyi-Kogan, G. S. 1999, *ApJ*, 514, 368
 Nelson, R. W., Salpeter, E. E., & Wasserman, I. 1993, *ApJ*, 418, 874
 Romanova, M. M., Ustyugova, G. V., Koldoba, A. V., & Lovelace, R. V. E. 2002, *ApJ*, 578, 420
 Ruffert, M. 1994a, *ApJ*, 427, 342
 Ruffert, M. 1994b, *A&AS*, 106, 505
 Shapiro, S. L., & Teukolsky, S. A. 1983, *Black Holes, White Dwarfs, and Neutron Stars* (New York: Wiley)
 Shvartsman, V. F. 1970, *Radiofiz.*, 13, 1852
 Stella, L., White, N. E., & Rosner, R. 1986, *ApJ*, 308, 669
 Toropin, Yu. M., Toropina, O. D., Savelyev, V. V., Romanova, M. M., Chechetkin, V. M., & Lovelace, R. V. E. 1999, *ApJ*, 517, 906
 Toropina, O. D., Romanova, M. M., Toropin, Yu. M., & Lovelace, R. V. E. 2003, *ApJ*, Submitted
 Treves, A., & Colpi, M. 1991, *A&A*, 241, 107
 Treves, A., Turolla, R., Zane, S., & Colpi, M. 2000, *PASP*, 112, 297
 Walter, F. M., & Lattimer, J. M. 2002, *ApJ*, 576, L45
 Wang, Y.-M., & Robertson, J. A. 1985, *A&A*, 151, 361
 Zhukov, V. T., Zabrodin, A. V., & Feodoritova, O. B. 1993, *Comput. Maths. Math. Phys.*, 33, 1099